Cement and Concrete Research 42 (2012) 447–458

Contents lists available at SciVerse ScienceDirect

Cement and Concrete Research

journal homepage: http://ees.elsevier.com/CEMCON/default.asp

Influence of the micro- and nanoscale local mechanical properties of the interfacial transition zone on impact behavior of concrete made with different aggregates

Savaş Erdem *, Andrew Robert Dawson, Nicholas Howard Thom

School of Civil Engineering, Faculty of Engineering, University of Nottingham, University Park, Nottingham NG7 2RD, UK

ARTICLE INFO

Article history:
Received 29 June 2011
Accepted 19 November 2011

Keywords:
Interfacial transition zone (B)
Mechanical properties (C)
Aggregate (D)
Concrete (E)
Microstructure (B)

ABSTRACT

The influence of the microscale local mechanical properties of the interfacial transition zone (ITZ) on macro-level mechanical response and impact behavior is studied for concretes made with copper slag and gravel aggregates. 3D nanotech vertical scanning interferometry, scanning electron microscopy coupled with energy dispersive X-ray micro-analysis, digital image analysis, and 3D X-ray computed tomography were used to characterize the microstructures and the ITZs. It was deduced that a stronger and denser ITZ in the copper slag specimen would reduce its vulnerability to stiffness loss and contribute to its elastic and more ductile response under impact loading. The analysis also indicated that a significant degeneration in the pore structure of the gravel specimen associated with a relatively weaker and non-homogeneous ITZ occurred under impact. Finally, it was also concluded that increased roughness of ITZ may contribute to the load-carrying capacity of concrete under impact by improving contact point interactions and energy dissipation.

1. Introduction

Concrete and structures in many civil engineering applications can often be subjected to a range of accidental or deliberate high-strain-rate loading, apart from static loading. The responses of concrete materials under such loads are quite different and several failure modes (perforation, scabbing, spalling and punching shear) can be observed [1]. It is generally observed that the strain corresponding to the peak stress under compression or the fracture strain (deflection) under flexural impact increases with increasing loading rate [2]. Nevertheless, the dynamic behavior of concrete materials under high-strain rate loading has still not fully been understood. For example, it is not yet clear what the physical origins of this strength increase are. In addition, the influence of the internal microstructure of concrete, and the mechanisms which cause different crack and failure patterns when varying the loading rate, remain open questions [3].

Development of advanced and effective inspection techniques during the last decade has demonstrated that the atomic level (nano and micro) properties of concrete has a profound effect upon its macro-level properties, and these structure–property relationships lie at the heart of modern concrete technology. Understanding structure–property relationships of concrete under different loading states is an essential yet challenging task for the concrete technologist. A massive amount of research is still going on to take a look behind the curtain and understand the mysteries behind the most popular construction material in today's world.

Concrete is a highly complex and non-homogeneous material, and its properties depend on the properties of the individual constituents [coarse aggregate, matrix and interfacial transition zone (ITZ) between the two] and the interactions between them [4]. It would not be an exaggeration to claim that the ITZ is the most mysterious region among the constituents for scientists in concrete technology. Prof. Karen Scrivener and her colleagues did pioneer work on the ITZ in concrete at the Imperial College London in the 80s, and they made a significant contribution to our current knowledge on that topic. The origin of the ITZ lies in the so called “wall” effect sourced by the aggregate particles, in which the aggregates will appear locally flat to the cement grains and disrupt their packing [5] or micro-bleeding effect which leads to the accumulation of mix water beneath the aggregates during vibration [6]. As a result of these effects, the ITZ is structurally inferior and contains much coarser pores, and easily cleavable and highly soluble CH crystals compared to the bulk cement paste [7]. But at that point, such a unique structure gives rise to the following key questions that need to be answered: To what extent does the existence of the ITZ has on any of the practical influences of the engineering properties of concrete or is it just a peculiarity of academic interest? [8]. Here, as stated by Wang et al. [9], there are two contrary opinions: On the one hand, some researchers [10,11] claim that since the ITZ is the weakest part of the micro-structural system and the place where cracking initiates; it plays a significant role on the mechanical and transport properties of concrete. On the other hand, some researchers [12] suggest that there is no obvious reason to assume that the ITZ might have significant negative effects

* Corresponding author. Tel.: +44 115 823 2424; fax: +44 115 951 3909.
E-mail address: evxse1@nottingham.ac.uk (S. Erdem).

0008-8846/$ – see front matter © 2011 Elsevier Ltd. All rights reserved.
doi:10.1016/j.cemconres.2011.11.015

on the permeance and mechanical performance of concrete, even for concrete with a w/c ratio of 0.50. The conflicting arguments from various resources indicate that the significance of the ITZ with regard to the overall concrete behavior, it seems, remains uncertain.

From a fracture mechanics standpoint, when the adhesive bonds between the aggregate and the matrix are damaged under applied loads, the concrete weakens, and cracks develop and propagate either through the particles or around them. The type of propagation influences the energy consumption and the interlocking effect, and plays a key role in concrete toughness [13]. This damage mechanism occurs at a nano or micro level. Research conducted so far is still too limited to answer the question of how do changes in the micro- and nano level properties of ITZ affect the overall concrete behavior. Moreover, to the authors' best knowledge; there has been no study to evaluate the influence of the local properties of the ITZ on concrete behavior under impact loading. An attempt was therefore made to investigate the changes in the strength and impact behavior of concrete associated with changes in the micromechanical properties of the ITZ regarding the influence of the characteristics of two types of coarse aggregate (uncrushed gravel and copper slag).These two aggregates were selected for three reasons. First, both have much higher particle strength than the paste so that the interfacial zone and its properties become of major importance for micro-level damage initiation and propagation. Secondly, they exhibit very different particle stiffness which is expected to result in different local stress concentration behaviors at the paste-aggregate interface. Thirdly, they have very different surface rugosity, likely having a difference in influence on the micro-level response at the aggregate-paste interface. Choosing copper slag has a further potential benefit in that, if successful, its use would help to address a small part of the global waste disposal problem. It should also be noted that in a previous paper, the authors have studied the influence of different surface roughness and porosity aggregates (uncrushed gravel and sintered fly ash) on the post-impact micro damage and strength properties of concrete.

2. Experimental methodology

2.1. Production of concrete mixtures

General purpose Portland-fly ash cement CEM II/B-V 32.5 R was used to produce all the concrete mixes. Local river sand with a specific gravity of 2.66 constituted the fine aggregate in all mixes. Two types of coarse aggregate ranging in size from 14 mm down to 4 mm were used in this study. The first type was uncrushed gravel sourced from a local quarry and the other was a copper slag, kindly provided by Hodge Clemco Ltd. The X-ray diffraction pattern of the copper slag is shown in Fig. 1. The observed peaks correlate well with the reference patterns for olivine and illite as the main phases present in the copper slag and indicate the copper slag to be well crystallized. In all mixes, the volume fractions of cement, coarse aggregate, sand and free water were the same. The only difference was the type of coarse aggregate used in the mixtures. The mix proportions are given in Table 1. The same volumetric percentages were selected for the copper slag and conventional aggregate to eliminate the effect of grading difference on concrete performance. All concrete mixtures were batched using a mechanical pan mixer, placed in oiled steel molds in two layers; each layer was compacted by using a vibrating table before being covered with plastic sheets. The specimens were left in their molds for 1 day before de-molding and cured at 20 ± 2 °C in a water tank until the day of testing.

Table 1
Mix proportions for 1 m³.

Material (kg/m³)	Gravel concrete	Copper slag concrete
Cement	330	330
Water	198	198
Sand	678	678
Gravel (coarse aggregate)	1115	0
Copper slag (coarse aggregate)	0	1620

2.2. Tests and analysis performed

2.2.1. Aggregate characterization

A digital image processing (DIP) technique was used to analyze the particle shape characteristics of the coarse aggregates. After acquiring the images, a computer software program (Image Pro^{+}™) was used for the quantification of aggregate shape characteristics. Surface roughness of the aggregates was measured by stylus profilometry using a 2D Mitutoyo Surftest SV 662 profiler with a 5 μm stylus. The physical properties of the aggregates were also determined based on standard procedures. Table 2 shows the physico-mechanical properties and geometrical parameters of the aggregates used. In general, the copper slag is much denser and has a higher strength than the

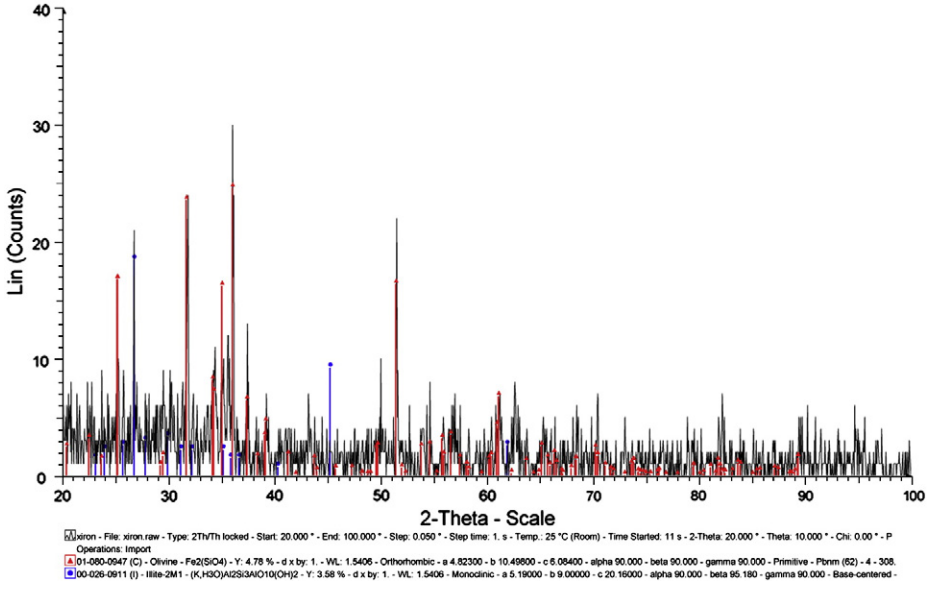

Fig. 1. X-ray diffraction pattern of the copper slag.

Table 2
The physico-mechanical properties of aggregates used.

Characteristics	Gravel	Copper slag
Specific gravity (Mg/m³)	2.65	3.75
Surface roughness — Sa (μm)	5.6	8.75
Angularity	1.12	1.17
Impact value (%)	12	8.3
Fractal dimension	1.08	1.02
The modulus of elasticity (GPa)	56.9	113.9

gravel. In addition, the copper slag has a much rougher surface texture and higher degree of angularity than the gravel.

2.2.2. Concrete tests

Four cubes (100×100×100 mm) were used to measure the compressive strengths of the mixtures in accordance with the relevant British European Standard. The dynamic modulus of elasticity of prismatic specimens was determined using a commercially available non-destructive ultrasonic device. The natural frequencies were calculated using the equation suggested by Zheng et al. [14]. The flexural strength was tested on 100×100×500 mm concrete beams with four-point flexural loading. This test was carried out using a closed-loop deflection controlled Zwick universal testing machine with a capacity of 200 kN at a constant deflection rate of 0.10 mm-min.

2.2.3. Impact testing

Impact tests were carried out using a Rosand type 5 instrumented falling weight impact tester shown schematically in Fig. 2. The impact machine is capable of dropping a 120 kg mass from heights of up to 3 m onto the target specimen. The specimen was placed vertically on a cylindrical steel base (diameter = 150 mm) located at the center of the impact machine, as shown in Fig. 2. The hammer was dropped from 500 mm height to provide a striking velocity of 3 m/s. An accelerometer attached to the impact hammer was used to measure acceleration and displacement during the impact process. Assuming that

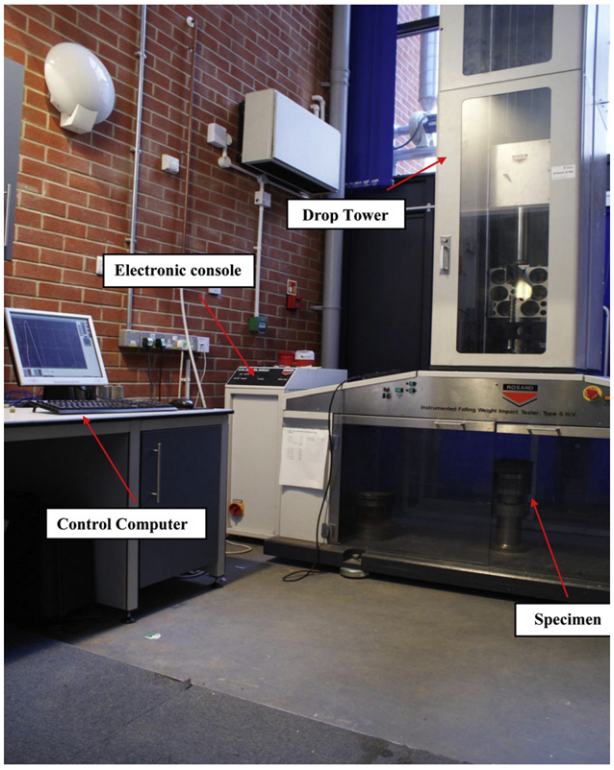

Fig. 2. Photograph of drop tower impact machine.

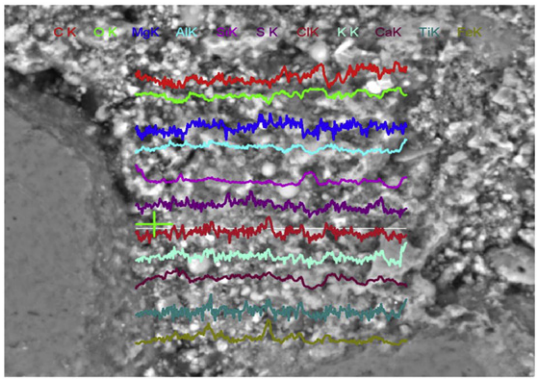

Fig. 3. Energy dispersive spectroscopy analysis in the ITZ.

the hammer displacement was essentially equal to that of the specimen surface, the velocity and the displacement of the specimen surface could be computed using the following equations [15]:

From the initial potential energy, the velocity of the impactor at the beginning of the impact event is

$$\dot{u}(0) = \sqrt{2gh} \tag{1}$$

where g is the corrected gravitational acceleration (91% of the true value) due to the friction in the hammer guide; h is the drop height.

At any time t during the impact, the velocity of the hammer is equal to

$$\dot{u}_h(t) = \dot{u}_h(0) + \int_0^t \dot{u}h(t)dt \tag{2}$$

where $\dot{u}_h(t)$ is the recorded acceleration by the accelerometer.

Then, the displacement of the hammer and the displacement of the specimen surface at any time t become

$$u_h(t) = \int_0^t \left[\dot{u}h(0) + \int_0^t \ddot{u}h(t)dt\right] \cdot dt. \tag{3}$$

The load-deformation and the deformation-time histories were also recorded using a high-speed data acquisition system. Four specimens of each mixture were tested.

2.2.4. Micro-mechanical properties of ITZ

2.2.4.1. Measurement of ITZ surface area roughness. The surface area roughness of the ITZs was measured using a vertical scanning interferometer (VSI)-Fogale Nanotech Photomap 3D, Ville Active, Nimes, France. The same concrete samples prepared for the SEM investigation were also used this analysis. A quantitative evaluation of

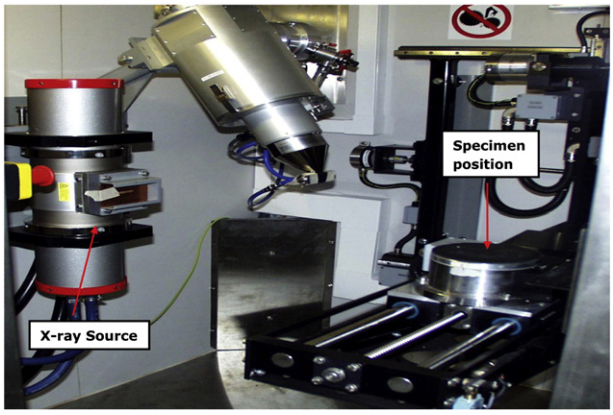

Fig. 4. X-ray CT system and its components.

each file was digitally carried out to calculate the area roughness — Sa (Arithmetic mean deviation of the surface). A mean value of five measurements was used as a response value for each experiment. It should be noted that to the best of our knowledge, this is the first time a VSI has been used for measuring ITZ roughness.

2.2.4.2. Measurement of ITZ micro-hardness (strength). Micro-hardness test can be used for evaluating the local mechanical response of material. Micro-strength is deduced from the micro-hardness, using an indenter/bearing capacity analysis [16–18]. A Vickers micro-hardness test was carried out to determine the micro-hardness in the transition zone between aggregates and hardened cement paste. The test load was selected to be 0.05 N in order to be able to map the ITZ and not to result in indentations that are hard to measure accurately [17]. The contact time was 10 s. The measured range was up to 100 μm away from the surface of aggregates. Ten determinations were performed on the surface of each sample.

2.2.4.3. Measurement of ITZ elemental composition. The SEM was fitted with an energy dispersive X-ray (EDX) spectrometer. X-ray line

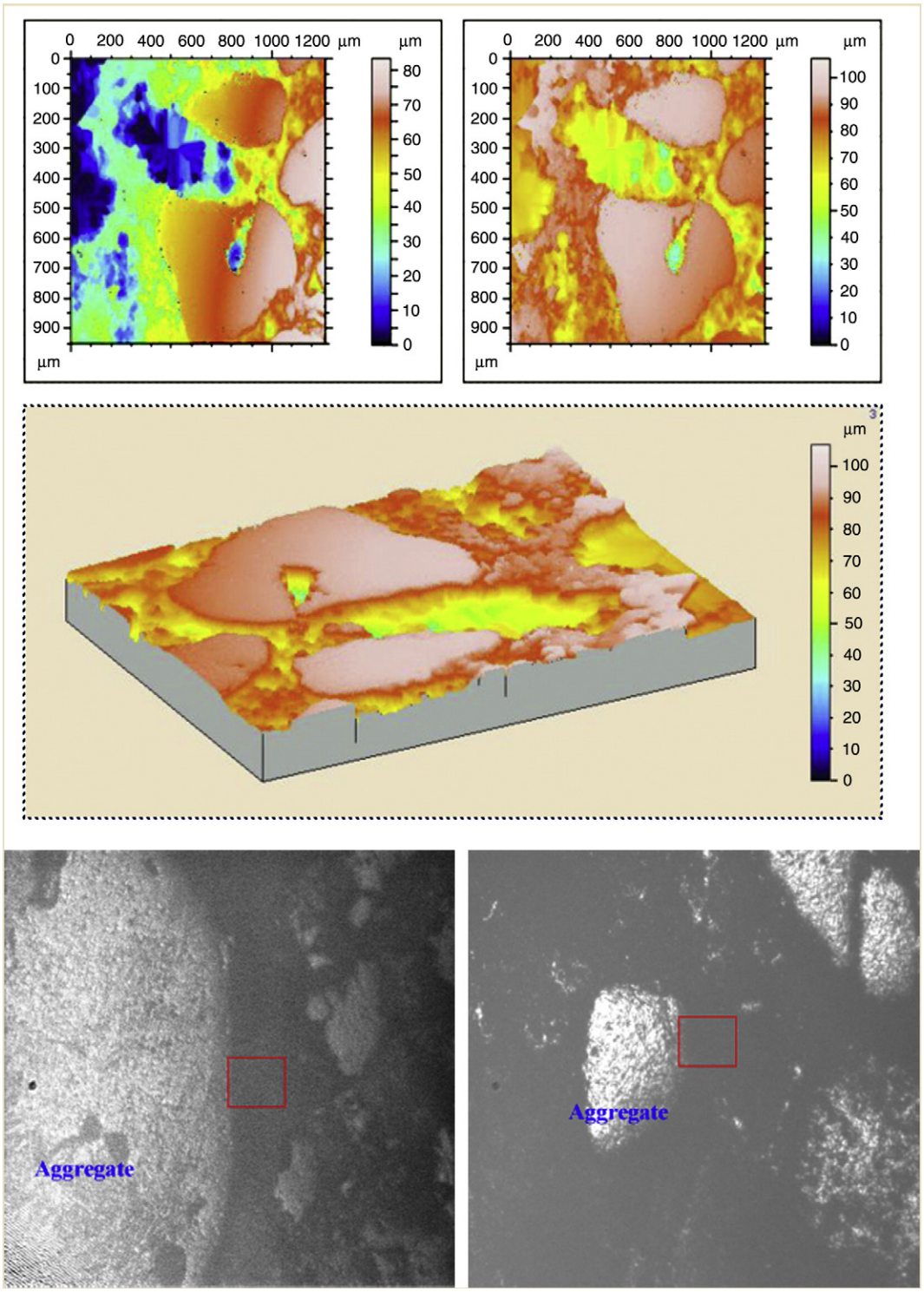

Fig. 5. Surface topography images and profile of the gravel specimen.

scanning analyses were made in the region of the aggregate-cement paste interfaces of the specimens to investigate the presence of various elements. An example of the analysis is given in Fig. 3. The counting rate for each analysis obtained was 100 s. The analysis was obtained between 5 and 20 μm from the aggregate interface. Trägårdh [19] used the following classification in order to distinguish hydrates rich in C–S–H, rich in calcium hydroxide (CH) and monosulfate (AFm). The same classification was used in this study.

$$\text{C–S–H} : 0.8 \le \text{Ca/Si} \le 2.5, (\text{Al} + \text{Fe})/\text{Ca} \le 0.2$$

$$\text{CH} : \text{Ca/Si} \ge 10, (\text{Al} + \text{Fe})/\text{Ca} \le 0.4, \text{S/Ca} \le 0.04$$

$$\text{AFm} : \text{Ca/Si} \ge 4, (\text{Al} + \text{Fe})/\text{Ca}\ 0.40, \text{S/Ca} > 0.15$$

2.2.4.4. Measurement of ITZ crack density. The ITZ micro-crack measurements after impact loading were obtained by means of a microscopic analysis. The captured images were processed and edited with image analysis software (Image J) to compute the crack length,

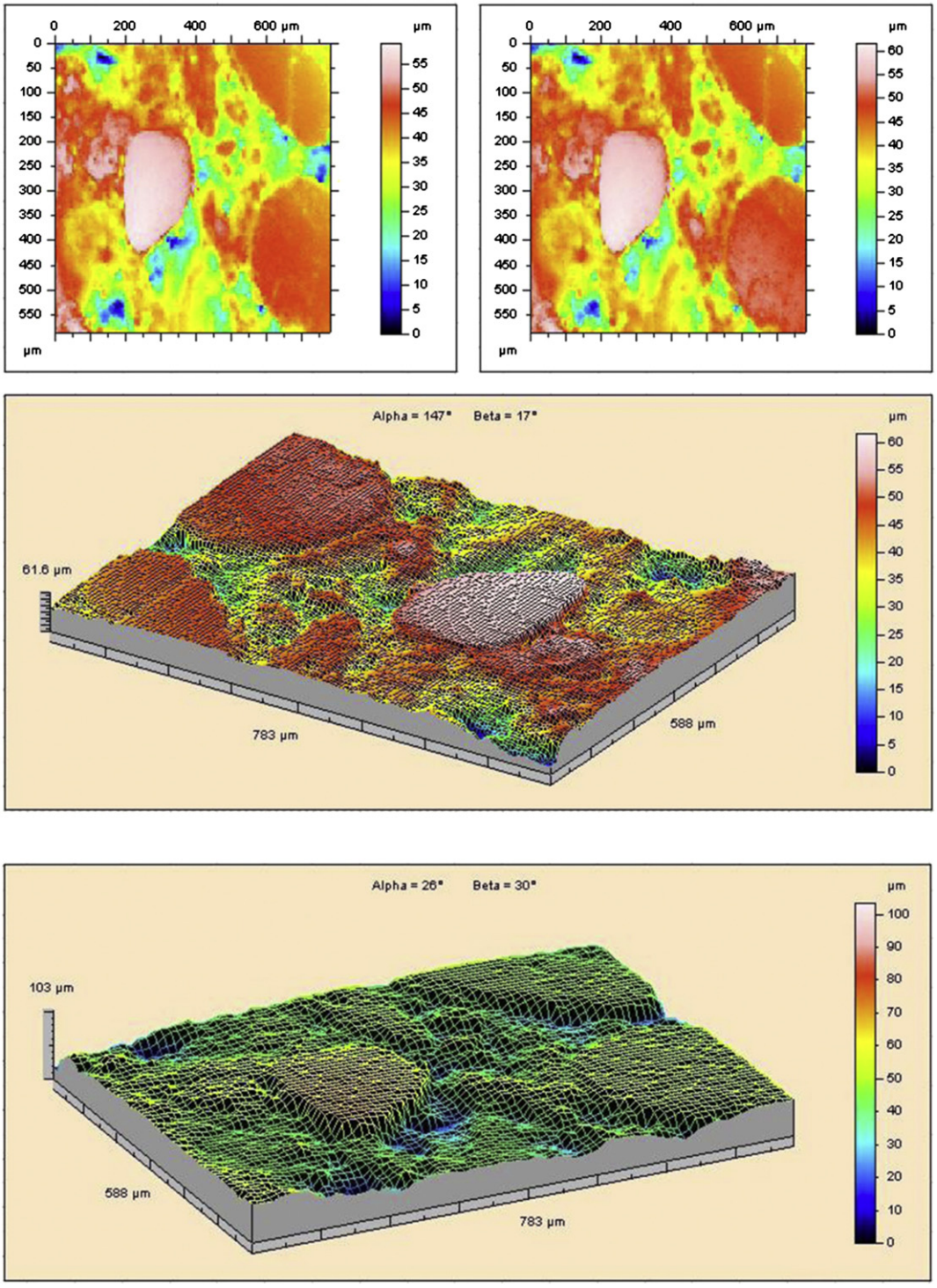

Fig. 6. Surface topography images and profile of the copper slag specimen.

crack width and crack density. The crack density (1/μm), equal to the micro-crack length per area unit, was calculated by dividing the total length of the cracks (μm) to the total examined surface area (μm^2).

2.2.5. X-ray CT investigation

In order to investigate the void characteristics of the mixtures, sequences of 2D images were captured through the height of the 100 mm cube specimens with a slice thickness of 1 mm using the non-destructive X-ray CT system. The system had a 350 kV X-ray source, and a line detector. The resolution of the X-ray CT images was approximately 0.21 mm/pixel which is about 120 pixels per inch (dpi). A picture of the X-ray CT system is shown in Fig. 4. The captured images from the X-ray CT system were then analyzed and converted to 3D images using the standard capabilities of an image analysis software package (Image J). Finally, the converted images were used to identify and quantify air voids within the specimen.

3. Results and discussion

3.1. Characterization of the ITZ

3.1.1. Surface area roughness of ITZ

The micrographs of the surfaces were constructed at a magnification which makes it possible to focus particularly on the interfacial zone near the aggregate particles in the images. This magnification resulted in a measurement area with dimensions of about 589×784 μm. From this area, the Sa values were measured.

Figs. 5 and 6 show the 2D top surface and 3D surface topography images, and the camera views for the ITZ of gravel and copper slag concrete, respectively. The calculated Sa roughness values are also illustrated in the figures. In general, the figures indicate the surface in the case of the gravel specimen may be approximated as a flat plane whereas the surface in the case of the copper slag specimen may provide significant perturbations. In addition, the area roughness (Sa = 7.35 μm) of the copper slag specimen is significantly lower than that of the gravel specimen (Sa = 3.41 μm). However, it is assumed that such topography in the copper slag specimen would affect its deformation behavior and energy absorption characteristics positively when the concrete is subjected to impact loading — this will be further discussed in a later section.

Rounded particles usually pack more closely than angular particulars [20]. This is because particle asperity breakage and/or significant dilation would be needed to achieve the same relative displacement of angular particles, and both of these need more energy than does the rolling or particle slip largely achieved in rounded aggregate mixes. Thus proper interlocking of angular aggregates is hindered, and this leads to a more random distribution of fine and coarse hydration products as well as cementitious particles which, in turn, may lead to an increase in the local capillary porosity in the hardened paste. This results in peaks and troughs of strength across the length of an aggregate-paste boundary.

3.1.2. Micro-hardness of ITZ

The average micro-hardness (strength) distribution measured in the ITZ of each mix was plotted against the distance from the aggregate surface in Fig. 7.

The results suggest that there are noticeable differences between the copper slag and gravel specimens. In the specimen manufactured with the copper slag, the micro-hardness at 50 μm away from the aggregate surface reached a level of 36 HV 0.01, whereas it was only 29 HV 0.01 for the gravel specimen. From a material science point of view, such behavior of the specimen prepared with the copper slag could be attributed to a higher crystallinite proportion in the copper slag aggregate. As stated by Perkins [21], increased crystallinite usually results in a higher yield stress and Young's modulus, and vice-versa. Thus, it could be expected that the inclusion of stiffer and denser material in the specimen would arise its micro-hardness value. It can also be suggested that densification of microstructure – likely due to the aggregate characteristics – strengthens the matrix by improving the contact point interactions in its constituents. However, it is interesting to note that when the micro-hardness of the cement paste is normalized, the gains of the slag disappear. It is well-known that the presence of rigid and well-bonded stiff inclusions (such as fiber and aggregate) or other inhomogeneities (such as large pores) can restrain the stress fields developed under the indenter, leading to an indentation size that is smaller than would be expected from the nature of the paste alone and thus, the hardness of the paste is expected to increase.

3.1.3. Chemistry of the hydrous phases in the ITZ

The average atomic ratios of the hydrous phases in the ITZ of the mixtures measured by SEM coupled with EDX are listed in Table 3. The analysis revealed that there was significant difference in the Ca/Si, (Al + Fe)/Ca and S/Ca ratios of the ITZs of the two concretes.

Significant differences in all three ratios existed between the analyses of intermixed nature. The intermixed phases in the ITZ in the

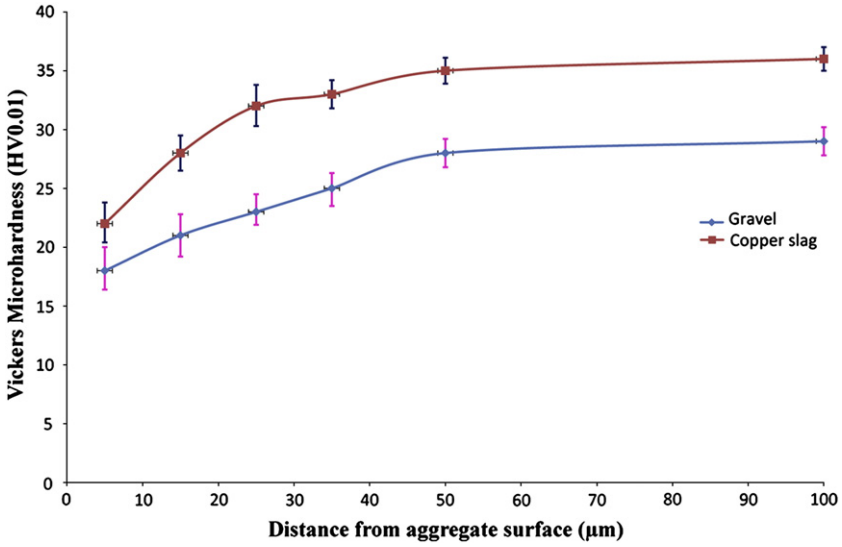

Fig. 7. Micro-hardness profiles of the specimens.

Table 3
Average atomic ratios of analyses in the ITZ of hydrous materials.

Concrete ID	ITZ (hydrous phases)	Ca/Si	(Al + Fe)/Ca	S/Ca
Gravel	Intermixed	2.66	0.34	0.041
Copper Slag	Intermixed	1.44	0.75	0.057

copper slag concrete had a lower Ca/Si but higher (Al + Fe)/Ca and S/Ca ratios. The ratios of (Al + Fe)/Ca and S/Ca indicate that the intermixed material in the copper slag concrete almost predominantly consisted of a monosulfate phase. Such a structure may promote secondary ettringite formation in the microstructure of the impact-damaged concrete. This will be further discussed in a later section.

3.2. Engineering properties

The basic engineering properties of the gravel and copper slag concrete are tabulated in Table 4. The results demonstrate that the compressive strength of concrete made with copper slag coarse aggregate was much higher than that of the conventional aggregate concrete. Caliskan and Behnood [22] reported that the compressive strength of copper slag coarse aggregate concrete was marginally higher than that of limestone aggregate concrete. Khanzadi and Behnood [23], on the other hand, reported that the incorporation of copper slag coarse aggregate increases the compressive strength by about 12% on average. The higher strength was mainly attributed to the strength characteristics of copper slag aggregates, and more importantly their porous and rough surface texture that may provide a superior bond and transition zone between the paste and aggregate. However, the authors did not perform any microstructural investigations or any quantitative assessment of the ITZ to prove their hypothesis.

Using the X-ray CT system along with digital image analysis techniques; aggregates, air voids and other constituents can be visualized and evaluated, and thus this can be used to study the structure/property relationships in concrete. Fig. 8 shows 3D images obtained by the X-ray technique coupled with digital image analysis corresponding to horizontal slices through 100 mm cube specimens at different heights. The calculated void content and average void size are also illustrated in the figure. The analysis shows that the inherent void distribution was not homogeneous for both specimens, and there were three distinct regions with respect to the void distribution: two low void content regions at the top and bottom, and one relatively high void content region in the middle part of the specimens. The figure also shows that the void content and average void size in the gravel concrete are higher than those in the copper slag concrete. In the authors' opinion, such initial defects and heterogeneous microstructure would lead to a significant increase in the destructive transverse tensile strains during the loading and the concentrations of the stresses around pores in which large pores would intensify the external loading. This, correspondingly, provides a line of weakness for failure to take place on, and accelerates crack growth and strain incompatibilities and, hence, facilitates fracture initiation and propagation associated with reduced failure surface energy.

In addition, the EDX analysis indicated a Ca/Si average ratio of 2.66 in the transition zone of the gravel specimen with an evidence of Al

Table 4
Engineering properties of the mixtures.

Concrete ID	Density (kg/m³)	Compressive strength (MPa)	Flexural tensile strength (MPa)	Dynamic modulus of elasticity (GPa)	Natural frequency-f (Hz)
Gravel	2325	25.4	4.00	41.0	340.5
Copper slag	2720	33.2	4.70	50.9	350.7

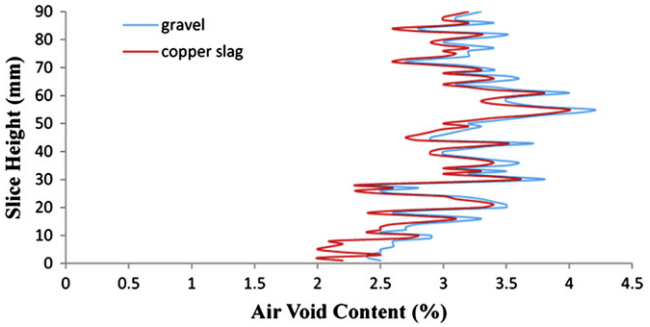

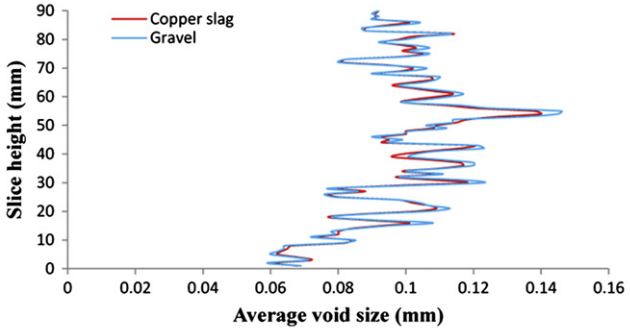

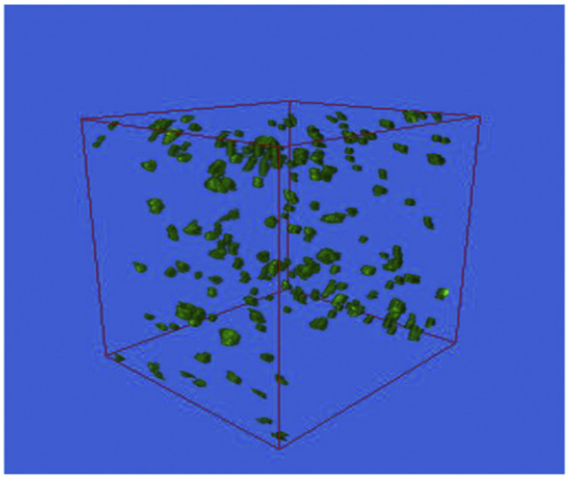

Fig. 8. 3D X-ray CT images of the specimens.

(Al = 8.10), signifying that the ITZ was a relatively porous and rich in ettringite but relatively poor in calcium silicate hydrates. This has been confirmed from microstructural investigations with SEM analysis, as shown in Fig. 9a and b. By contrast, the analysis shows a Ca/Si average ratio of 1.44 in the transition zone of the copper slag specimen, indicating a more homogenous microstructure of the matrix in the ITZ by means of fewer portlandite crystals and most likely, less AFt/m phases intermixed with C–S–H. It is supposed that such internal structure of the ITZ in the gravel specimen would support damage mechanism by decreasing the integrity of the concrete by reducing the connected area for the matrix materials that flow and deform in the vicinity of the coarse aggregate and by reducing the adhesion between particles and mortar, which, in turn, ultimately reduce the strength.

The concrete mixture prepared with copper slag aggregate exhibited about 25% higher dynamic modulus of elasticity than the concrete containing gravel aggregate. This is assumed to be because of relatively lower internal vibration damping properties in the material. The mortar matrix with copper slag is less porous and has a higher density compared to the reference mortar matrix, and thus the ultrasonic pulse can move faster there. As expected due to the

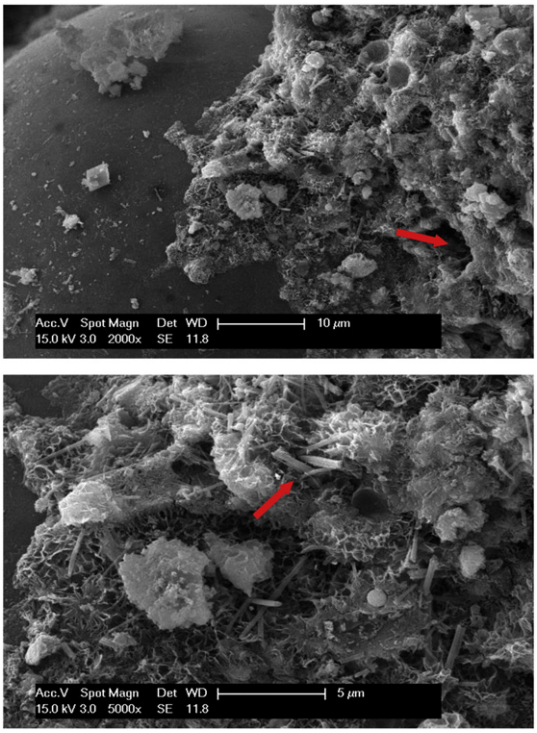

Fig. 9. Interfacial morphology of the gravel specimen.

high interfacial bond strength, the flexural strength is observed to be higher for the copper slag concrete than for the gravel concrete.

3.3. Behavior under impact

Since parameters such as the velocity and mass of the hammer, shape of the hammer nose, thickness of the concrete disks and boundary conditions of the concrete disks etc. were fixed, the resistance of the concrete disks to impact loading is assumed to be mainly related to the mechanical properties of the concrete disks themselves, which are basically a function of the coarse aggregate used for this study.

Fig. 10 shows load-time histories (all histories relate to the average of at least four samples for each mix) for both gravel and copper slag concrete during the first drop of impact. It is observed that in the first cycle of wave propagation, the magnitude of load for the copper slag specimen is much higher than that of the gravel specimen. The peak value of load is 17.2 kN compared to a peak load of 11.8 kN in the gravel concrete. It can be concluded that the impact resistance is strongly related to the stiffness of the material. As mentioned in Section 3.1.2, higher crystallinite usually results in a higher yield stress and Young's modulus and vice versa. Under the light of this theory, when the specimen is subjected to high rates of loading, the copper slag with larger stress capability acts as a barrier to crack propagation and reduces relaxation of plastic strain incompatibilities, which in turn could impose (relatively) large deviations of cracks to the interfaces between the particle and the matrix where there is already a strong ITZ providing much larger distances between the cracks (holding energy) and thus the specimen will be able to withstand more loading. It should also be mentioned that observation of the fractured surfaces indicates that a relatively higher percentage of the copper slag aggregates was pulled from their cavities, and the failure surface is more tortuous in the case of copper slag concrete. By contrast, the relative percentage of broken coarse aggregate was higher in the gravel concrete specimen.

Table 5
Micro-crack density of the ITZ.

Concrete ID	Maximum crack width (μm)	Total crack length (μm)	Total crack area (μm²)	Crack density (1/μm)
Copper slag	28.90	705.9	9360.6	0.075
Gravel	24.80	978.1	15422.5	0.062

The concentration of microcracks in the ITZ could be an important parameter to understand the damage process of the specimen subjected to impact loading and support the theory presented above. Table 5 shows the measured crack densities in the ITZ of the mixtures. As can be seen from Table 5, the occurred damage in the ITZ of the copper slag concrete was more extensive compared to that of the gravel concrete. As highlighted by Akcaoglu et al. [4], the bigger the difference between the strengths of the ITZ and the surrounding matrix, the higher the tendency of micro-cracking in the ITZ. So, it is supposed that the relatively bigger incompatibility between the ITZ and mortar strength in the case of copper slag concrete could possibly force the cracks to accumulate in the transition zone even under high loading rates. At that point, it is also worth mentioning the presence of the deposit of the ettringite needles in air voids of the impact-damaged specimen, as illustrated in Fig. 11. It is supposed that the chemical composition of the ITZ (i.e. release of sulfate or high amount

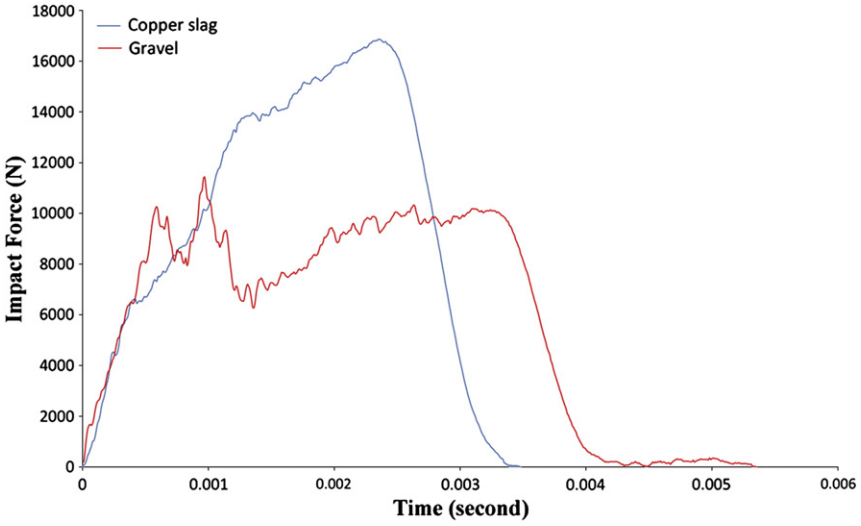

Fig. 10. Load-time histories of the specimens during the first drop of impact.

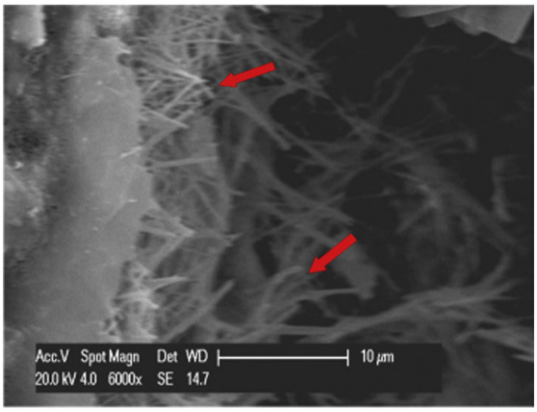

Fig. 11. Air void partially filled with ettringite crystals in the damaged concrete.

of Al, Fe and S) – see Table 3 – may promote ettringite re-crystallization (secondary ettringite formation) but unfortunately, the results cannot answer the question of whether their formations contributed to the damage. It is common to see ettringite in the voids and cracks of deteriorated concrete [24] but so far, there is no clear evidence that the ettringite crystals are the cause of crack formation.

Another possible reason could be the higher interfacial surface roughness of the copper slag specimen, as highlighted in Section 3.1. As it is concluded by Zampini et al. [25], the paste-aggregate interface can toughen the paste by increasing its roughness, which in turn may result in an increase in toughness of the concrete. Overall, an increased interfacial roughness may enhance the material strength against the angle of frictional resistance by improving the contact point interactions and may increase the area needed to be created on the surface during fracture, and thus the concrete can withstand a high level of load and consume more energy.

The load–displacement histories of the specimens during the first drop of impact are presented in Fig. 12. Interestingly, the ascending branch of the load–deflection curves of the specimens is both irregular and highly non-linear (most obvious in the gravel concrete). This could be attributable to the reflections of the stress waves from the specimen boundaries and their interactions, and the anisotropic nature of concrete itself [26] or presumably, generation of compression shock waves during impact would accelerate interlinking and dissipation of micro pores and other flaws in the contact area of the paste matrix by highly perturbed stress fields. This, in turn, may weaken the bond at the paste-aggregate interface and may further increase the plastic anisotropy. In addition, it can also be thought that the shock waves may interact with the secondary stress waves generated by structural inhomogeneities in the case of the gravel specimen and further increase the magnitude of damage.

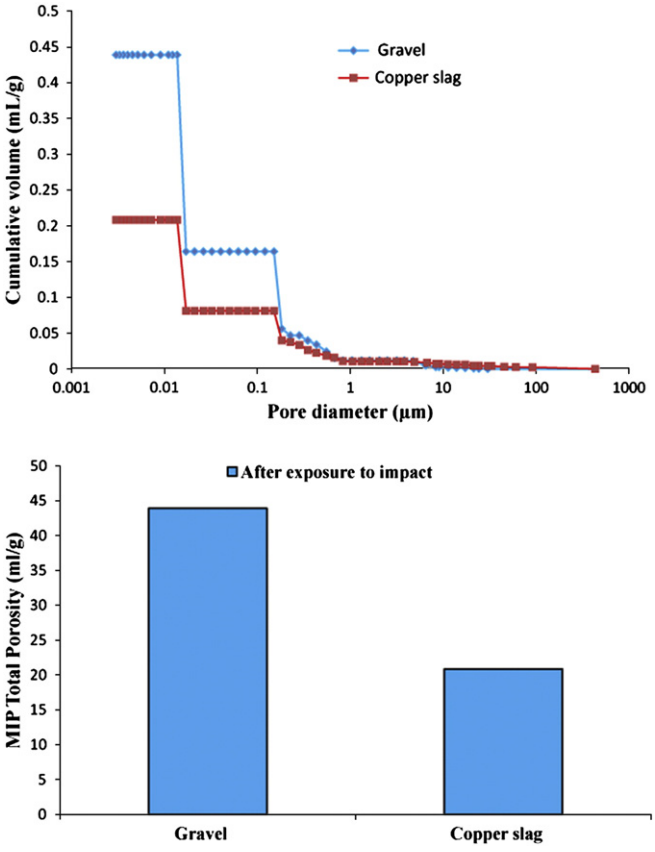

Fig. 13. Pore size distribution of the specimens after subjected to impact.

Fig. 13 shows the pore size distribution and pore volume of the specimens obtained by using a mercury intrusion porosimeter after being subjected to impact, and provides strong support for the aforementioned opinion. From the figure, it can be seen that the cumulative volume vs. pore diameter curve for the copper slag specimen

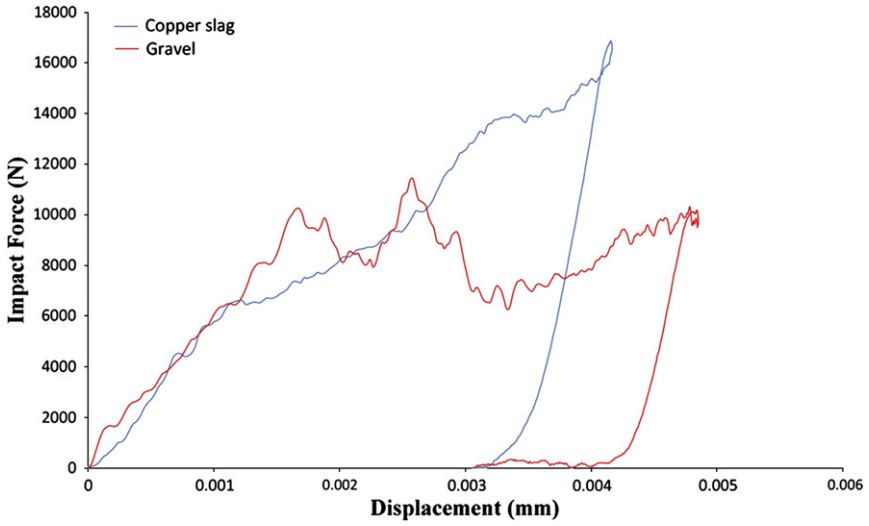

Fig. 12. Load–displacement histories of the specimens during the first drop of impact.

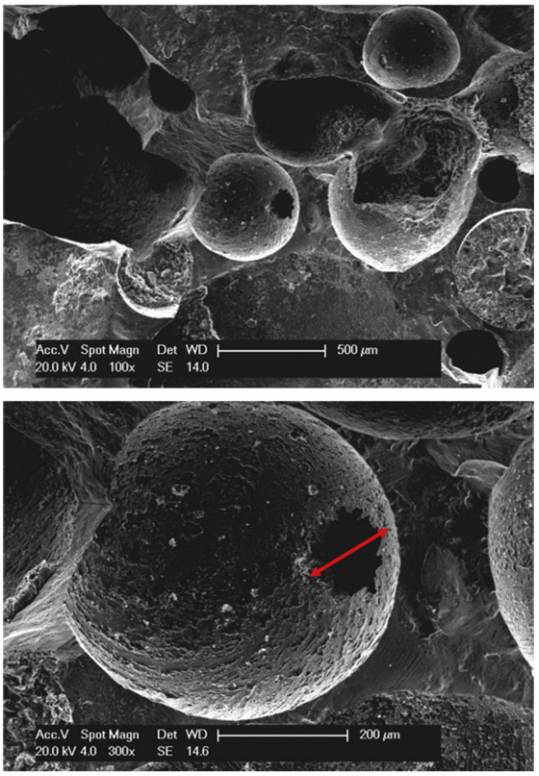

Fig. 14. Low-resolution image of air voids (a) and high-resolution images of air void showing openings in air-void layer.

was quite different from that of the gravel specimen. For the gravel specimen, the peaks of the cumulative volume was much larger than that of the copper slag specimen and the highest peak occurred within a range of 0.10 to 0.15 μm, signifying that the impact enlarged the micro pore diameter and, caused clustering and coarsening the interconnected pores. The coalescence of pores will inevitably reduce effective interparticle contact area on the fracture surfaces, which is undesirable under dynamic conditions because much of the imparted energy is normally lost in plastic deformations [27]. The microscopic analysis (see Fig. 14) seems to confirm the openings in the air void layers. It should also be noted that the formation of small fragments also justifies that cracks may effectively deviate to adjacent transition zones in the case of the copper slag specimen as mentioned in the previous paragraph.

It is also interesting to note that the reflection time taken for the compression stress waves to travel from the impact point to the bottom of the gravel specimen was almost twice that of the copper slag specimen or in other words, the copper slag specimen responded more quickly upon impact loading, and thus it showed more elastic features than the gravel specimen. This could be attributed to the fact that as mentioned in Section 3.1, the gravel specimen has a weaker interface accompanied by a non-homogeneous microstructure in the presence of the internal flaws around the transition zone. Hence, these inherent characteristics would possibly cause a delay in the travel time of the shock waves.

The load–displacement histories of the specimens in each impact are also recorded and illustrated in Figs. 15 and 16 for the gravel and copper slag specimen, respectively. As can be observed from the figure, the copper slag specimen exhibits much larger deformation before fracture. This confirms that the response of concrete under impact is quite different. In the static condition, modification of concrete usually diverts the fracture path from the ITZ to the aggregate, as in high-strength concrete, producing a destructive brittle failure. However, it is seen that in the dynamic condition, the load is carried by the aggregate and transferred to the interface. A strong interface in the case of the copper slag specimen would have a higher ability to redistribute stress accompanied by (relatively) higher energy dissipation, and ultimately a more ductile failure has taken place. Fig. 12 also shows strong support for this behavior. Here, the specimens exhibited elasto-viscoplastic behavior when the load was removed (most pronounced in the gravel specimen), possibly leading to generation of larger stress perturbations at the interface. Correspondingly, a weaker interface having a lower ability to redistribute stress would contribute to the comparatively sudden failure.

We believe that there is another important point that must be highlighted. It is found that the rate of curve peak decrease is better controlled in the copper slag specimen. For example, the curve peak of the 2nd impact is higher than the peak of the 1st–3rd impacts, and just before the failure (at the fourth drop), the amplitude of load significantly increased. By contrast, surprisingly, the peak of the final (third) drop in the gravel specimen was even higher than the curve peaks of the first and second impact (incremental collapse). As is well-known, an increase in the applied loading triggers anisotropic damage and crack propagation within the mix, leading to a reduction in structural stiffness which alters the resonant frequency of vibration of the specimen. As the natural frequency of vibration has

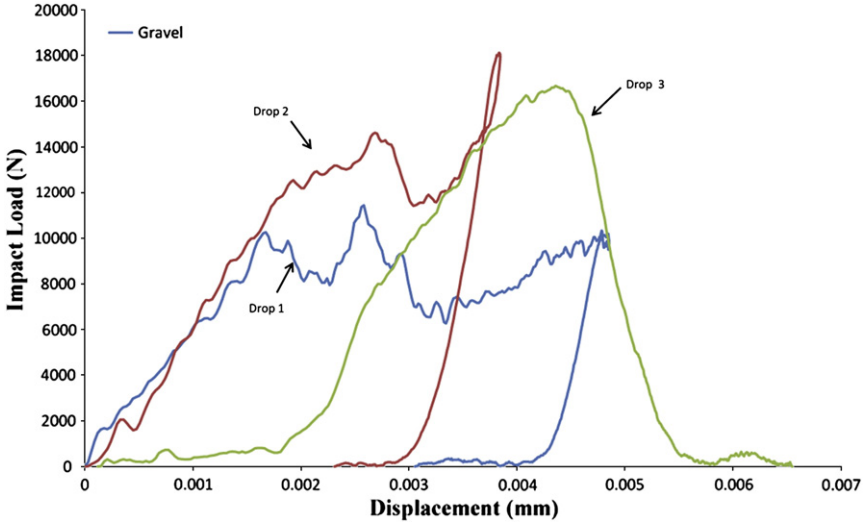

Fig. 15. Load–displacement histories of the gravel specimen in each impact cycle.

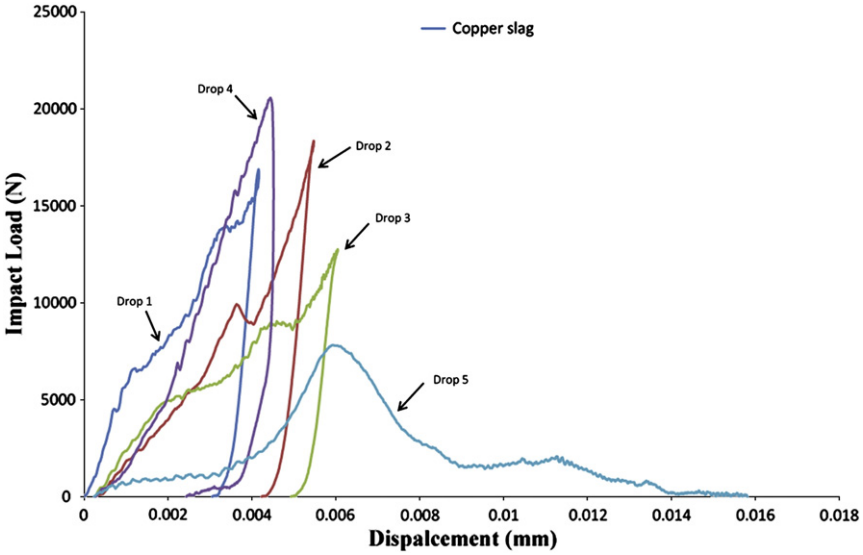

Fig. 16. Load–displacement histories of the copper slag specimen in each impact cycle.

an inverted ratio with the mass, the load increases with the decrease in the natural frequency. However, at this point the difference between the behavior of the two specimens gives rise to the question: Why is the influence of the natural frequency shown more clearly in the gravel specimen? This is possible due to the fact that a relatively weaker interfacial zone associated with micro-cracks and other internal flaws in the gravel specimen makes it more vulnerable to stiffness loss under the applied load as recently proposed by Rao et al. [28] for the behavior of recycled aggregate concrete under impact.

The crack pattern and failure surfaces of disk specimens for both gravel and copper slag concretes are presented in Fig. 17a and b, respectively. The failure patterns shows that the failure was usually initiated by a radial tensile crack at or near the impact point and then the cracks propagated sideways, eventually breaking the specimens into several pieces, as shown in Fig. 17a and b.

4. Concluding remarks

The following conclusions can be drawn from the work presented in this paper:

- Much denser, stronger and rougher, and higher crystallinite copper slag aggregate produced a dense, stronger and much rougher ITZ, which in turn provides more resistance to impact.
- The copper slag concrete showed a more ductile and elastic response as well as less vulnerability to stiffness loss under impact likely due to a stronger and dense ITZ, and more homogeneous microstructure. By contrast, impact stress waves may possibly interact with secondary stress waves generated by structural inhomogeneities leading to a more pronounced damage in the gravel specimen.
- An ITZ with higher surface roughness may result in a higher load-carrying capacity of concrete by contributing to more energy dissipation within the mixture, and thus more resistant to impact. The chemical elemental composition of the ITZ may promote the secondary ettringite formations in the voids of the damaged specimen.
- The variation of pore structure can reflect the deterioration of concrete subjected to impact loading. The pore structure of the gravel specimen was more deteriorated under impact loading. Coarsening or interaction and coalescence of pores would lead to the reduction in the area of particle–particle contact on the fracture surface.
- Concrete with copper slag aggregate had a much higher compressive strength than the concrete made with gravel aggregate partly due to the strength characteristics of the aggregate and partly due to the high Ca/Si ratio through the ITZ and more homogeneous internal structure of the concrete (as confirmed by the X-ray CT, EDX and image analysis). In addition, its flexural tensile strength was higher than the corresponding value of the gravel concrete as a result of the higher bond strength.

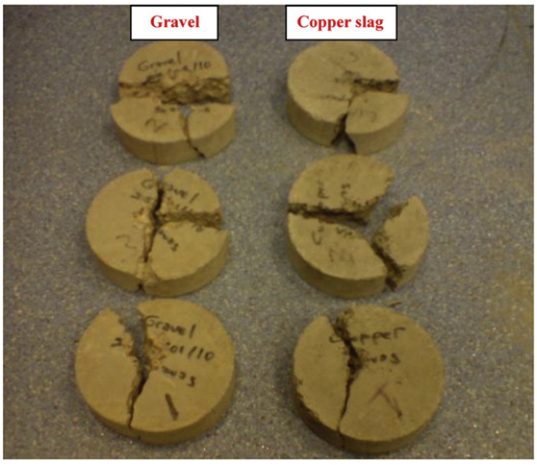

Fig. 17. Crack patterns and failure surfaces of the disk specimens.

Acknowledgments

The authors would like to gratefully acknowledge Dr. Kevin Anthony Brown and Dr. Nigel Neate (University of Nottingham) for their valuable help and comments during the impact tests and the XRD analysis. Special thanks must also go to Dr. M.T. Bassuoni (University of Nottingham) for the input of helpful discussion and advice. The authors also wish to thank Mr. Darek Bridger, who is the managing director of Hodge Clemco Ltd., for providing the copper slag aggregates.

References

[1] J.F. Georgin, J.M. Reynouard, Modelling of structures subjected to impact: concrete behaviour under high strain rate, Cement Concr. Compos. 25 (2003) 131–143.
[2] L. Zhang, Impact resistance of high-strength fiber-reinforced concrete, PhD Thesis, University of British Columbia, 2008.

[3] L. Snozzi, A. Caballero, J.F. Molinari, Influence of the meso-structure in dynamic fracture simulation of concrete under tensile loading, Cem. Concr. Res. 41 (2011) 1130–1142.
[4] T. Akçaoğlu, M. Tokyay, T. Çelik, Assessing the ITZ micro-cracking via scanning electron microscope and its effect o the failure behaviour of concrete, Cem. Concr. Res. 35 (2005) 358–363.
[5] K.L. Scrivener, A.K. Crumbie, P. Laugesen, The interfacial transition zone (ITZ) between the cement paste and aggregate in concrete, Interface Sci. 12 (2004) 411–421.
[6] A. Goldman, A. Bentur, Effects of pozzolanic and non-reactive micro fillers on the transition zone in high-strength concretes, in: J.C. Maso (Ed.), Proceedings of the RILEM International Conference (Toulouse) Proceedings 18, Interfaces in Cementitious Composites, E & FN Spon, London, 1992, pp. 53–61.
[7] J.P. Ollivier, J.C. Maso, B. Bourdette, Interfacial transition zone in concrete, Adv. Cem. Based Mater. 2 (1995) 30–38.
[8] A. Bentur, M.G. Alexander, D. Bentz, O. Buyukozturk, J. Elsen, D. Hooton, H. Jennings, A. Katzs, K.O. Kjellsen, A. Kronlof, B. Laggerblad, S. Mindess, J.P. Ollivier, K. Scrivener, J. Skalny, et al., Review of the work of the RILEM TC 159-ETC: engineering of the interfacial transition zone in cementitious composites, Mater. Struct. 33 (2000) 82–87.
[9] X.H. Wang, S. Jacobsen, J.Y. He, Z.L. Zhang, S.F. Lee, Application of nanoindentation testing to study of the interfacial transition zone in steel fiber reinforced mortar, Cem. Concr. Res. 39 (2009) 701–715.
[10] K.M. Nemati, P.J.M. Monterio, K.L. Scrivener, Analysis of compressive stress-induced cracks in concrete, ACI Mater. J. 95 (1998) 617–630.
[11] H.S. Wong, M. Zobel, N.R. Buenfield, R.W. Zimmerman, Influence of the interfacial transition zone and micro-cracking on the diffusivity, permeability and sorptivity of cement-based materials after drying, Mag. Concr. Res. 61 (2009) 571–589.
[12] S. Diamond, J. Huang, The ITZ in concrete — a different view based on image analysis and SEM observations, Cement Concr. Compos. 23 (2001) 179–188.
[13] G.V. Guinea, K. El-Sayed, C.G. Rocco, M. Elices, J. Planas, The effects of the bond between the matrix and the aggregates on the cracking mechanism and fracture mechanism of concrete, Cem. Concr. Res. 32 (2002) 1961–1970.
[14] L. Zheng, X.S. Huo, Y. Yuan, Experimental investigation on dynamic properties of rubberized concrete, Const. Build. Mater. 22 (2008) 939–947.
[15] P. Sukontasukkul, P. Nimityongskul, S. Mindess, Effect of loading rate on damage of concrete, Cem. Concr. Res. 34 (2004) 2127–2134.
[16] W. Zhu, P.J.M. Bartos, Application of depth-sensing micro-indentation testing to study of interfacial zone in reinforced concrete, Cem. Concr. Res. 30 (2000) 1299–1304.
[17] S. Igarashi, A. Bentur, S. Mindess, Micro-hardness testing of cementitious materials, Adv. Cem. Based Mater. 4 (1996) 48–57.
[18] M. Sonebi, Utilization of micro-indentation technique to determine the micro-mechanical properties of ITZ in cementitious materials, Proceedings of ACI Session on “Nanotechnology of Concrete: Recent Developments and Future Perspectives” November 7, 2006, Denver – USA, 2006.
[19] J. Trägárdh, Microstructural features and related properties of self compacting concrete, in: A. Skarendahl, O. Petersson (Eds.), Proceedings of the First International RILEM Symposium on Self Compacting Concrete, RILEM, Cachan, Cedex, 1999, pp. 175–186.
[20] A.K.H. Kwan, C.F. Mora, Effects of various shape parameters on packing of aggregate particles, Mag. Concr. Res. 53 (2001) 91–100.
[21] W.G. Perkins, Polymer toughness and impact resistance, Polym. Eng. Sci. 39 (1999) 2445–2460.
[22] S. Caliskan, A. Behnood, Recycling copper slag as coarse aggregate: hardened properties of concrete. In: Proceedings of seventh international conference on concrete technology in developing countries, (2004): 91–98.
[23] M. Khanzadi, A. Behnood, Mechanical properties of high-strength concrete incorporating copper slag as coarse aggregate, Const. Build. Mater. 23 (2009) 2183–2188.
[24] M.D.A. Thomas, T. Ramlochan, Field cases of delayed ettringite formation, in: K. Scrivener, J. Skalny (Eds.), International RILEM TC 186- ISA Workshop (Villars) on Internal Sulphate Attack and Delayed Ettringite Formation, 2002, pp. 85–97.
[25] D. Zampini, H.M. Jennings, S.P. Shah, Characterization of the paste-aggregate interfacial transition zone surface roughness and its relationship to the fracture toughness of concrete, J. Mater. Sci. 30 (1995) 3149–3154.
[26] S. Mindess, L. Zhang, Impact resistance of fibre-reinforced concrete, P. I. Civil Eng-Str B. 162 (2009) 69–76.
[27] P.D. Hallett, A.R. Dexter, J.P.K. Seville, Identification of pre-existing cracks on soil-fracture surfaces using dye, Soil Tillage Res. 33 (1995) 163–184.
[28] M.C. Rao, S.K. Bhattacharyya, S.V. Barai, Behaviour of recycled aggregate concrete under drop weight impact load, Const. Build. Mater. 25 (2011) 69–80.